

DYNAMO EFFECT IN MHD TURBULENT CHANNEL FLOW

Fujihiro Hamba

Institute of Industrial Science,
University of Tokyo
Komaba, Meguro-ku, Tokyo, 153-8505, Japan
hamba@iis.u-tokyo.ac.jp

ABSTRACT

The generation of large-scale magnetic field due to small-scale motion of a conducting fluid, which is called the dynamo action, is important in understanding magnetic fields in astro/geophysical objects and in controlled fusion devices. A large eddy simulation (LES) of magnetohydrodynamic (MHD) turbulent channel flow is carried out and turbulent statistics are obtained to investigate the dynamo effect. It is shown that a streamwise mean magnetic field is generated due to the effect of the turbulent electromotive force. It is suggested that the cross-helicity dynamo effect contributes to the turbulent electromotive force; that is, the electromotive force parallel to the mean vorticity is generated due to the turbulent cross helicity. The dynamo effect is also investigated using the transport equations for the turbulent kinetic and magnetic energies.

INTRODUCTION

The behavior of the magnetic field in the earth and the sun and in the plasma controlled fusion devices is closely related to the motion of a conducting fluid such as the molten iron and the plasma gas. In the MHD flows at high magnetic Reynolds numbers turbulent motions enhance the diffusion effect of the magnetic field like the scalar transport in the non-MHD turbulent flows. However, the turbulent diffusion effect cannot account for the large-scale magnetic field actually observed in astro/geophysical phenomena and in engineering devices. It is expected some dynamo effect exists which drives and sustains the large-scale magnetic field against the diffusion effect. The α dynamo is the most famous dynamo mechanism (Krause and Rädler, 1980). Helical fluid motions drive the electromotive force in the direction of the mean magnetic field. On the other hand, the cross-helicity dynamo was also proposed and investigated. The electromotive force is driven in the direction of the mean vorticity when the cross-helicity, the correlation between the velocity and the magnetic field, has non-zero value (Yoshizawa, 1998).

In the induction equation for the mean magnetic field, the turbulent electromotive force appears as an unknown

term. In order to close the magnetic field equation, the term needs to be modeled using the mean field. The mean field dynamo theory has been studied theoretically and numerically; for example the dynamo mechanism for the solar magnetic field is investigated in detail (Brandenburg and Subramanian, 2005). On the other hand, a turbulence theory called the two-scale direct-interaction originally developed for non-MHD flows was extended and applied to the MHD turbulence (Yoshizawa, 1998). Using this theory, several turbulence models were proposed to investigate the magnetic field in astrophysical objects and in plasma controlled fusion devices (Yoshizawa et al., 2003; Yokoi et al., 2008). However, these models are not fully assessed using experiment and numerical simulations in contrast to the turbulence models for the non-MHD flow. The direct numerical simulation (DNS) and LES are useful tools for validating the models. Several three-dimensional simulations for solar dynamo have been carried out. These simulations involve fairly complex physical phenomena such as the thermal convection, the fluid compressibility, and the gravity effect. More simple simulations must be useful as a first step.

In this work, we carry out an LES of MHD turbulent channel flow. Mean fields and turbulent statistics are obtained to examine the dynamo mechanism and to assess the MHD turbulence model.

MODEL EQUATIONS AND NUMERICAL METHOD

In this paper we adopt Alfvén velocity units such as $\mathbf{b}/\sqrt{\rho\mu_0} \rightarrow \mathbf{b}$. The equations for the grid scale (GS) velocity and magnetic fields are given by

$$\frac{\partial \bar{\mathbf{u}}}{\partial t} = -\nabla \cdot (\bar{\mathbf{u}} \bar{\mathbf{u}} - \bar{\mathbf{b}} \bar{\mathbf{b}}) - \nabla \cdot \boldsymbol{\tau} - \nabla(\bar{p} + \frac{1}{2} \bar{\mathbf{b}}^2) + \nu \nabla^2 \bar{\mathbf{u}} \quad (1)$$

$$\nabla \cdot \bar{\mathbf{u}} = 0 \quad (2)$$

$$\frac{\partial \bar{\mathbf{b}}}{\partial t} = -\nabla \times \bar{\mathbf{e}}, \quad \bar{\mathbf{e}} = -\bar{\mathbf{u}} \times \bar{\mathbf{b}} - \mathbf{e}_M + \lambda_M \bar{\mathbf{j}}, \quad \bar{\mathbf{j}} = \nabla \times \bar{\mathbf{b}}, \quad (3)$$

$$\nabla \cdot \bar{\mathbf{b}} = 0 \quad (4)$$

where ν is the viscosity and λ_M is the magnetic diffusivity. The subgrid scale (SGS) stress $\boldsymbol{\tau}$ and the SGS electromotive force \mathbf{e}_M are defined as

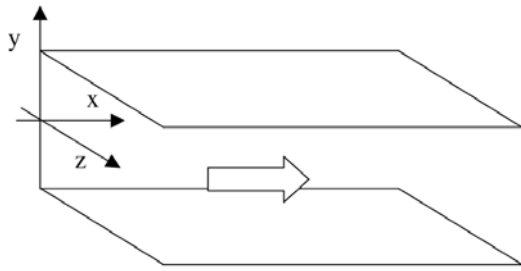


Figure 1. Computational domain of channel flow.

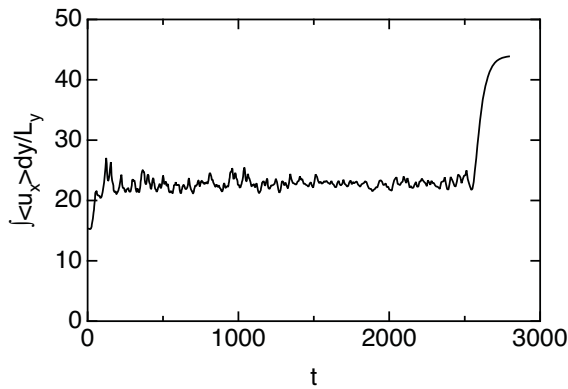


Figure 2. Time history of flow rate.

$$\boldsymbol{\tau} = \overline{\mathbf{u}\mathbf{u}} - \overline{(\mathbf{u}\mathbf{u} - \mathbf{b}\mathbf{b})} \quad (5)$$

$$\mathbf{e}_M = \mathbf{u} \times \mathbf{b} - \overline{\mathbf{u} \times \mathbf{b}} \quad (6)$$

As the SGS model we adopt the following model

$$\tau_{ij} = \frac{1}{3} \tau_{kk} \delta_{ij} - \nu_{SGS} \overline{s}_{ij}, \quad \overline{s}_{ij} = \frac{\partial \overline{u}_i}{\partial x_j} + \frac{\partial \overline{u}_j}{\partial x_i} \quad (7)$$

$$\mathbf{e}_M = -\lambda_{SGS} \overline{\mathbf{J}} \quad (8)$$

$$\nu_{SGS} = C_\nu \Delta^2 (\frac{1}{2} C_\nu \overline{s}_{ij}^2 + C_\lambda \overline{J}_i^2)^{1/2} \quad (9)$$

$$\lambda_{SGS} = C_\lambda \Delta^2 (\frac{1}{2} C_\nu \overline{s}_{ij}^2 + C_\lambda \overline{J}_i^2)^{1/2} \quad (10)$$

where $C_\lambda = (5/7)C_\nu$ and $C_\nu = 0.046$. This SGS model was derived by extending the Smagorinsky model for non-MHD turbulence to MHD (Hamba, 1989). It was assumed that the SGS viscosity and diffusivity can be expressed in terms of the SGS energy dissipation and the filter width Δ and that the production and dissipation terms are balanced to each other in the equation for the MHD SGS energy. The values of model constants are determined considering the theoretical value of the turbulent magnetic Prandtl number (Yoshizawa, 1998) and the correspondence to the Smagorinsky model in the non-MHD limit.

Using the above equations we carry out an LES of MHD channel flow driven by a constant pressure gradient $-dp_0/dx$. The computational domain is $L_x \times L_y \times L_z = 16\pi \times 2 \times (4/3)\pi$ and the number of grid points is $N_x \times N_y \times N_z = 256 \times 64 \times 64$ where x , y , and z denote the streamwise, wall-normal, and spanwise directions, respectively as shown in Fig. 1. The length scale

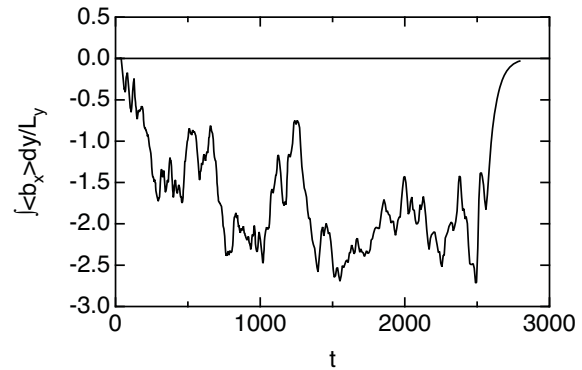


Figure 3. Time history of magnetic flux

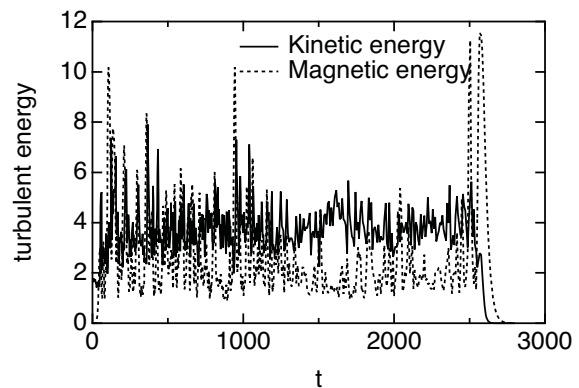


Figure 4. Time history of turbulent kinetic and magnetic energies.

is normalized by the channel half width $L_y/2$ and the velocity and magnetic fields are normalized by the friction velocity $u_\tau = (|dp_0/dx|L_y/2)^{1/2}$. The Reynolds and magnetic Reynolds numbers based on the friction velocity are set to $Re_\tau = 180$ and $Rm_\tau = 180$, respectively. The periodic boundary conditions are imposed in the x and z directions. The non-slip condition is adopted at the walls at $y = \pm 1$ for the velocity; the wall is treated as an insulator for the magnetic field. A statistical steady velocity field of the non-MHD turbulent channel flow is used as the initial condition for the velocity at $t=0$. A random seed field with zero mean is used as the initial condition for the magnetic field. Unlike the Hartman flow, the wall-normal component of the mean magnetic field B_y is set to zero. This is because we want to realize the turbulent field without the mean-field electromotive force $(\mathbf{U} \times \mathbf{B})_z$, which drives the mean field B_x in a trivial manner.

TEMPORAL EVOLUTION

First we examine the temporal evolution of the turbulent field. Figures 2 and 3 show the time history of volume average of the velocity and magnetic fields given by $(1/L_y) \int \langle \overline{u}_x \rangle_{xz} dy$ and $(1/L_y) \int \langle \overline{b}_x \rangle_{xz} dy$, respectively, where $\langle \cdot \rangle_{xz}$ denotes the x - z plane average. The time is

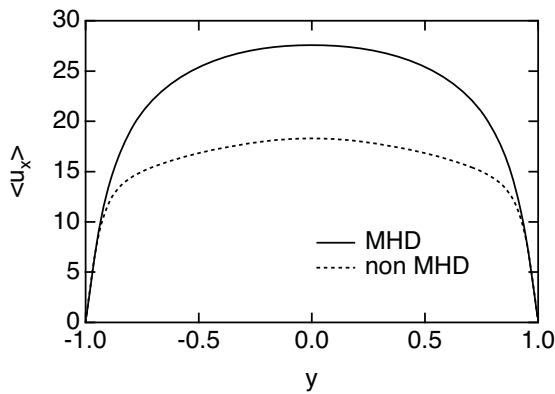


Figure 5. Mean velocity.

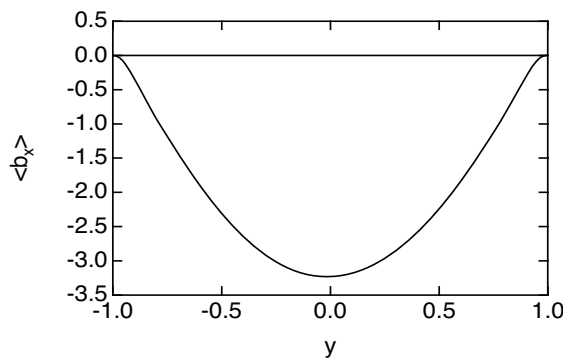


Figure 6. Mean magnetic field.

normalized by $(L_y/2)/u_\tau$. The mean velocity increases to about 22 at $t=100$ and a statistically steady state is kept until $t=2600$. On the other hand, the mean magnetic field shows negative values; it fluctuates in time. After $t=2600$ the turbulent fluctuations decrease to zero and the mean velocity shows a laminar profile.

Figure 4 shows the time history of volume average of the turbulent kinetic and magnetic energies given by $(1/L_y) \int \langle \bar{u}_i'^2 \rangle_{xz} dy$ and $(1/L_y) \int \langle \bar{b}_i'^2 \rangle_{xz} dy$. The turbulent energies fluctuate in time and are also sustained until $t=2600$. Therefore, it is shown that for a long time period until $t=2600$ an MHD turbulent field with a negative mean magnetic field is sustained.

TURBULENCE STATISTICS

In this section the statistical quantities are obtained by averaging over the x - z plane and in time from $t=1200$ to 2400. This average is denoted by $\langle \cdot \rangle$; the physical quantity is decomposed as $f = \langle f \rangle + f''$. Some mean values are also denoted by upper-case letters such as U_i and B_i .

Figure 5 shows the mean velocity profiles. The solid line is the present MHD result and the dashed line is the result of DNS of non-MHD channel flow of Moser et al. (1999). The mean velocity in the MHD case is fairly greater than that of the non-MHD case. Figure 6 shows the profile of the mean magnetic field. Although its magnitude is about

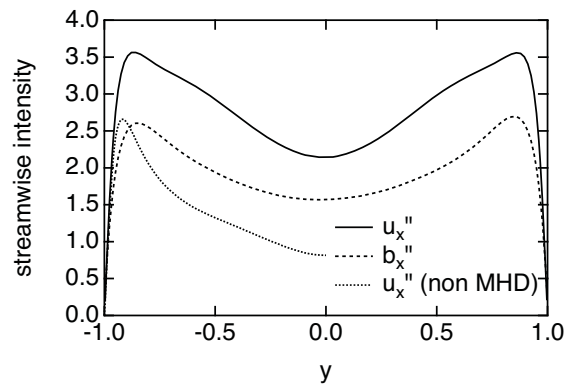


Figure 7. Streamwise component of turbulent intensity.

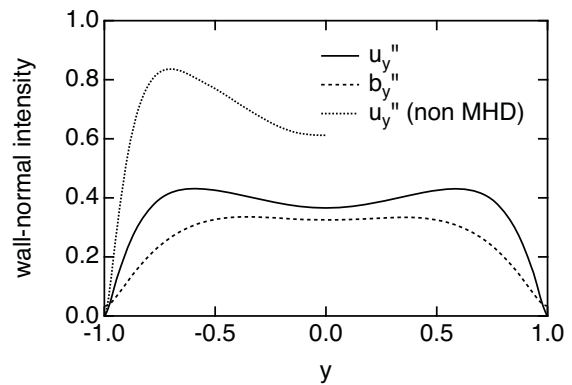


Figure 8. Wall-normal component of turbulent intensity.

10% of the mean velocity, it clearly shows a non-zero profile. It takes a peak value at the channel center. This profile cannot be explained in a simple manner because the mean-field electromotive force vanishes as mentioned before. Other runs with different initial random field show positive mean magnetic field (not shown here).

Figure 7 shows the streamwise component of the turbulent intensities $\langle \bar{u}_x'^2 \rangle^{1/2}$ and $\langle \bar{b}_x'^2 \rangle^{1/2}$. The velocity fluctuation in the MHD case is fairly greater than that in the non-MHD case. The magnetic-field fluctuation is slightly less than the velocity fluctuation. Figure 8 shows the wall-normal component of the turbulent intensities $\langle \bar{u}_y'^2 \rangle^{1/2}$ and $\langle \bar{b}_y'^2 \rangle^{1/2}$. The wall-normal component of the velocity fluctuation in the MHD case is less than that in the non-MHD case in contrast to the streamwise component. Therefore, the anisotropy of the turbulent intensity in the MHD case is greater than in the non-MHD case.

The mean velocity is driven by a constant pressure gradient. To understand the reason for the increase in the flow rate, we examine the balance of the mean momentum given by

$$\langle \bar{u}_x' \bar{u}_y'' \rangle + \langle \tau_{xy} \rangle - \nu \frac{\partial \langle \bar{u}_x \rangle}{\partial y} = y \quad (11)$$

Figure 9 shows four terms appearing in (11), the GS, SGS, viscous terms and the total stress; the GS stress term in non-MHD case is also plotted. Since a statistically steady state is

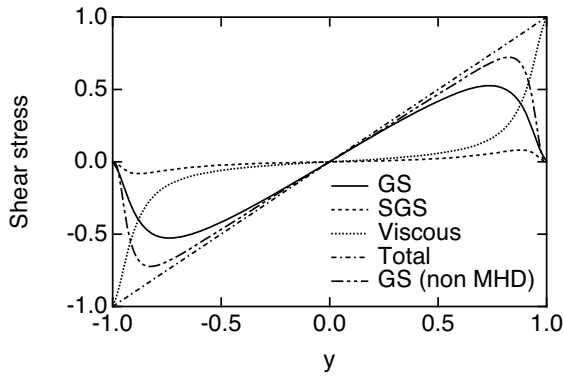


Figure 9. Balance of shear stress.

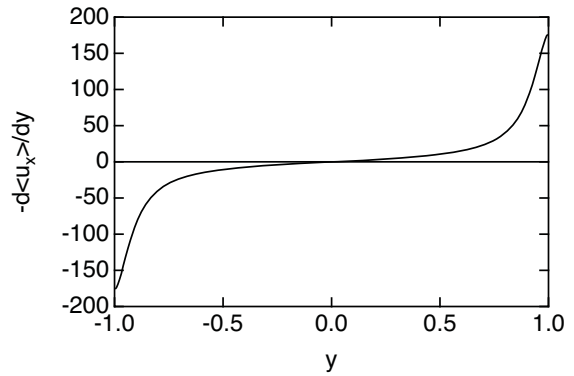


Figure 11. Mean vorticity.

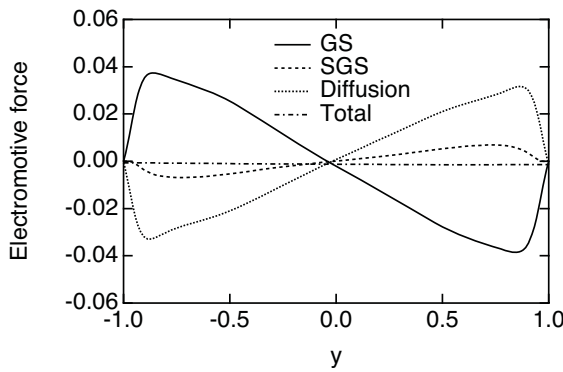


Figure 10. Balance of electromotive force.

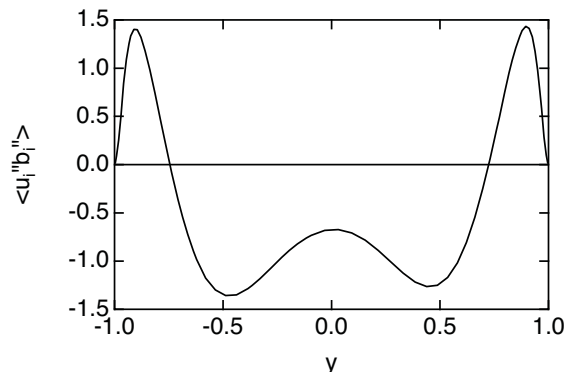


Figure 12. Turbulent cross helicity.

achieved, the total value is nearly equal to y . The magnitude of the GS stress $\langle \bar{u}_x' u_y'' \rangle$ is smaller than that in the non-MHD case. This is because the wall-normal velocity fluctuation $\langle \bar{u}_y'^2 \rangle$ is smaller in the MHD case as shown in Fig. 8. The small value of the wall-normal fluctuation is mainly due to the decrease in the redistribution effect by the pressure-strain term in the turbulent kinetic energy equation. This will be examined later.

On the other hand, the mechanism of the sustainment of the magnetic field shown in Fig. 6 is not trivial. The mean induction equation and the balance of the electromotive force are given by

$$\frac{\partial B_x}{\partial t} = -\frac{\partial \langle \bar{e}_z \rangle}{\partial y} \quad (12)$$

$$-\langle \bar{e}_z \rangle = \langle \bar{\mathbf{u}}'' \times \bar{\mathbf{b}}'' \rangle_z + \langle e_{Mz} \rangle - \lambda_M J_z \quad (13)$$

where $\mathbf{J} = \nabla \times \mathbf{B}$. Since the initial condition with $B_y = 0$ was set, there is no mean electromotive force $(\mathbf{U} \times \mathbf{B})_z$. Figure 10 shows four terms, the GS, SGS, molecular diffusion terms and the total electric field given by (13). Since a very long time average is taken, the total electric field $\langle \bar{e}_z \rangle$ is nearly zero. At $-0.8 < y < 0.8$ the SGS term $\langle e_{Mz} \rangle$ and the molecular diffusion term $-\lambda_M J_z$ show positive gradient. This gradient means the diffusion effect because it leads to a positive value of $\partial B_x / \partial t$ in (12) and to a decrease of the magnitude of B_x . On the other hand, the GS term $\langle \bar{\mathbf{u}}'' \times \bar{\mathbf{b}}'' \rangle_z$ shows negative gradient. This means a

dynamo effect that drives the mean magnetic field against the diffusion effect.

The turbulent electromotive force can be modeled as

$$\langle \mathbf{u}'' \times \mathbf{b}'' \rangle_z = \alpha B_z - \beta J_z + \gamma \Omega_z \quad (14)$$

where $\boldsymbol{\Omega} = \nabla \times \mathbf{U}$, α is the alpha coefficient related to the helicity $\langle \mathbf{u}'' \cdot \boldsymbol{\omega}'' \rangle$, β is the turbulent diffusivity, and γ is the cross-helicity dynamo coefficient (Yoshizawa, 1998). Since B_z and $\langle \mathbf{u}'' \cdot \boldsymbol{\omega}'' \rangle$ are small in the present flow, the alpha dynamo seems irrelevant. The β term simply enhances the diffusion. The mean vorticity $\Omega_z = -\partial U_x / \partial y$ shows negative (positive) value at $-1 < y < 0$ ($0 < y < 1$) in Fig. 11. The cross helicity $\langle \mathbf{u}'' \cdot \mathbf{b}'' \rangle$ shows negative value at $-0.7 < y < 0.7$ in Fig. 12. Therefore, the cross-helicity dynamo term shows negative gradient and can account for the GS electromotive force shown in Fig. 10. This result suggests that the cross helicity dynamo $\gamma \Omega_z$ is important in the present MHD turbulence.

ENERGY TRANSFER

In order to better understand the dynamo effect, we examine the transport equations for the turbulent kinetic and magnetic energies. The equations for the three components of the turbulent kinetic energy are given by

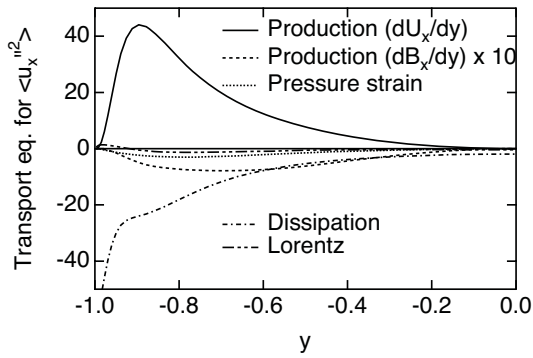


Figure 13. Transport equation for streamwise component of turbulent kinetic energy.

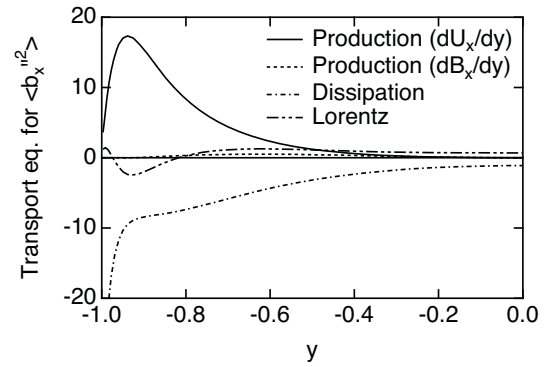


Figure 15. Transport equation for streamwise component of turbulent magnetic energy.

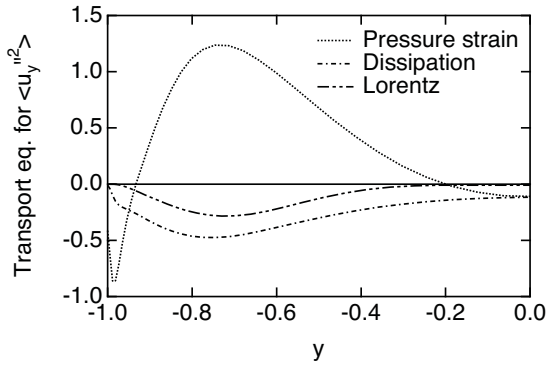


Figure 14. Transport equation for wall-normal component of turbulent kinetic energy.

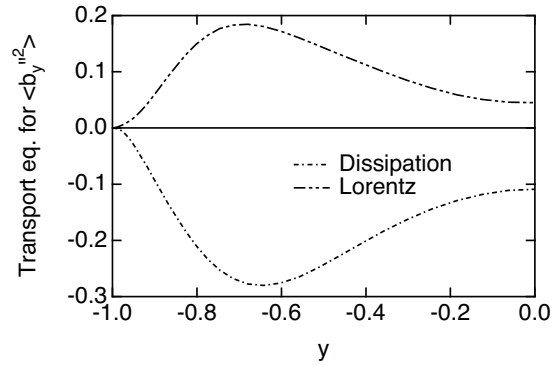


Figure 16. Transport equation for wall-normal component of turbulent magnetic energy.

$$\begin{aligned} \frac{\partial}{\partial t} \langle \bar{u}_x''^2 \rangle = & -2 \langle \bar{u}_x'' \bar{u}_y'' \rangle \frac{\partial U_x}{\partial y} + 2 \langle \bar{u}_x'' \bar{b}_y'' \rangle \frac{\partial B_x}{\partial y} \\ & + 2 \left\langle \bar{p}_M'' \frac{\partial \bar{u}_x''}{\partial x} \right\rangle - \epsilon_x + 2 \left\langle \bar{u}_x'' \bar{b}_k'' \frac{\partial \bar{b}_k''}{\partial x_k} \right\rangle + \dots \end{aligned} \quad (15)$$

$$\frac{\partial}{\partial t} \langle \bar{u}_y''^2 \rangle = 2 \left\langle \bar{p}_M'' \frac{\partial \bar{u}_y''}{\partial y} \right\rangle - \epsilon_y + 2 \left\langle \bar{u}_y'' \bar{b}_k'' \frac{\partial \bar{b}_k''}{\partial x_k} \right\rangle + \dots \quad (16)$$

$$\frac{\partial}{\partial t} \langle \bar{u}_z''^2 \rangle = 2 \left\langle \bar{p}_M'' \frac{\partial \bar{u}_z''}{\partial z} \right\rangle - \epsilon_z + 2 \left\langle \bar{u}_z'' \bar{b}_k'' \frac{\partial \bar{b}_k''}{\partial x_k} \right\rangle + \dots \quad (17)$$

where diffusion terms are omitted. The right-hand side of (15) consists of the two production terms, the pressure-strain term, the dissipation term, and the Lorentz term. The production term involving the mean velocity gradient represents the energy transfer between $\langle \bar{u}_x''^2 \rangle$ and U_x^2 whereas the production term involving the mean magnetic-field gradient represents the energy transfer between $\langle \bar{u}_x''^2 \rangle$ and B_x^2 . The Lorentz term corresponds to the energy transfer between $\langle \bar{u}_x''^2 \rangle$ and $\langle \bar{b}_x''^2 \rangle$. The production terms are involved only in (15) whereas the Lorentz terms appear also in (16) and (17).

Figure 13 shows the terms in the $\langle \bar{u}_x''^2 \rangle$ equation. Like those in the non-MHD case, the mean-shear production and dissipation terms are dominant as the energy gain and loss, respectively. The pressure-strain term shows a small

negative value, which represents the energy transfer to the other components of the turbulent kinetic energy. Its magnitude relative to the dissipation is small compared to the non-MHD case; this small value accounts for the strong anisotropy of the turbulent kinetic energy $\langle \bar{u}_i''^2 \rangle$. In the MHD case, the production term involving the mean magnetic-field gradient and the Lorentz term newly appear. We should note that the magnetic production term shows a negative value. This means the energy transfer from $\langle \bar{u}_x''^2 \rangle$ to B_x^2 and corresponds to the dynamo effect.

Figure 14 shows the terms in the $\langle \bar{u}_y''^2 \rangle$ equation. Since there is no production term, the pressure-strain term acts as the energy gain. Both the dissipation and Lorentz terms show negative value; the latter represents the energy transfer from $\langle \bar{u}_y''^2 \rangle$ to $\langle \bar{b}_y''^2 \rangle$.

The equations for the three components of the turbulent magnetic energy is given by

$$\begin{aligned} \frac{\partial}{\partial t} \langle \bar{b}_x''^2 \rangle = & 2 \langle \bar{b}_x'' \bar{b}_y'' \rangle \frac{\partial U_x}{\partial y} - 2 \langle \bar{b}_x'' \bar{u}_y'' \rangle \frac{\partial B_x}{\partial y} \\ & - \epsilon_{Mx} + 2 \left\langle \bar{b}_x'' \bar{b}_k'' \frac{\partial \bar{b}_k''}{\partial x_k} \right\rangle + \dots \end{aligned} \quad (18)$$

$$\frac{\partial}{\partial t} \langle \bar{b}_y''^2 \rangle = -\epsilon_{My} + 2 \left\langle \bar{b}_y'' \bar{b}_k'' \frac{\partial \bar{b}_k''}{\partial x_k} \right\rangle + \dots \quad (19)$$

$$\frac{\partial}{\partial t} \langle \bar{b}_z''^2 \rangle = -\epsilon_{Mz} + 2 \left\langle \bar{b}_z'' \bar{b}_k'' \frac{\partial \bar{u}_z''}{\partial x_k} \right\rangle + \dots \quad (20)$$

where diffusion terms are omitted. The last terms on the right-hand sides are the Lorentz term representing the energy transfer from the kinetic to magnetic energies. In these equations there is no pressure-strain term.

Figure 15 shows the terms in the $\langle \bar{b}_x''^2 \rangle$ equation. Like the $\langle \bar{u}_x''^2 \rangle$ equation the mean-shear production and dissipation terms are dominant. In this case, the production term involving the mean magnetic-field gradient shows a positive value, which represents the energy transfer from B_x^2 to $\langle \bar{b}_x''^2 \rangle$.

Figure 16 shows the terms in the $\langle \bar{b}_y''^2 \rangle$ equation. Instead of the pressure-strain term, the Lorentz term acts as the energy gain. It is shown that the $\langle \bar{b}_y''^2 \rangle$ component is sustained by the energy transfer from the kinetic energy $\langle \bar{u}_y''^2 \rangle$.

CONCLUSIONS

An LES of MHD turbulent channel flow was carried out using a Smagorinsky-type SGS model. It was shown that the mean magnetic field is driven by the turbulent electromotive force. The cross helicity dynamo is suggested to be important in the balance of the electromotive force. The transport equations for the turbulent kinetic and magnetic energies were also examined. The energy transfer from the turbulent kinetic energy to the mean magnetic field is confirmed. We expect that this simulation is useful for better understanding the dynamo mechanism in MHD turbulence.

REFERENCES

- Brandenburg, A., and Subramanian, K., 2005, "Astrophysical magnetic fields and nonlinear dynamo theory," *Phys. Rep.*, Vol. 417, pp. 1-209.
- Hamba, F., 1989, "Numerical simulation of reversed field pinches using a turbulence model," *J. Phys. Soc. Jpn.*, Vol. 58, pp. 2414-2422.
- Krause, F., and Rädler, K.-H., 1980, *Mean-Field Magnetohydrodynamics and Dynamo Theory*, Pergamon, Oxford.
- Moser, R. D., Kim, J., and Mansour, N. N., 1999, "Direct numerical simulation of turbulent channel flow up to $Re_\tau = 590$," *Phys. Fluids*, Vol. 11, pp. 943-945.
- Yokoi, N., Rubinstein, R., Yoshizawa, A., and Hamba, F., 2008, "A turbulence model for magnetohydrodynamic plasmas," *J. Turbulence*, Vol. 9, No. 37, pp. 1-25.
- Yoshizawa, A., 1998, *Hydrodynamic and Magnetohydrodynamic Turbulent Flows: Modelling and Statistical Theory*, Kluwer.
- Yoshizawa, A., Itoh, S.-I., and Itoh, K., 2003, *Plasma and Fluid Turbulence: Theory and Modelling*, IOP Publishing.